Solid Freeform Fabrication 2017: Proceedings of the 28th Annual International Solid Freeform Fabrication Symposium – An Additive Manufacturing Conference
Reviewed Paper

CASTING - FORGING - MILLING COMPOSITE ADDITIVE MANUFACTURING THECHNOLOGY

Haiou Zhang*, Runsheng Li*, Rui Wang*, Youheng Fu*, Xiangping Wang* ,
Guilan Wang†, and Shangyong Tang†

*State Key Laboratory of Digital Manufacturing Equipment and Technology, Huazhong University of Science and Technology,Wuhan, China, 430000
†State Key Laboratory of Materials Processing and Die and Mould Technology, Huazhong University of Science and Technology, Wuhan, China, 430000

Abstract

The current metal additive manufacturing has some drawbacks, such as poor performance in producing forgings, low accuracy and efficiency, and high cost. This paper proposes a new technology called casting-forging-milling composite (CFMC) additive manufacturing, which uses the efficient and cheap arc as the heat source. Synchronous arc welding and continuous semi-solid in-situ forging is achieved with micro-roller. Milling is incorporated into this process to remove defects and complete the part. Workpieces with equiaxed fine-grained microstructure and better performance than forgings have been obtained using CFMC. Testing shows that the mechanical performance exceeds the standards for forgings and most indicators are above the average levels. Trial products include titanium alloy aeronautical parts, a stainless steel propeller, and an aero-engine transition section which has passed the European standard x-ray inspection and test. The streamlined and low-cost manufacturing process achieved by using metal wire, integrated equipment and low pressure makes CFMC a green manufacturing model.

Introduction

Conventional machinery manufacturing has several serious weaknesses. First, it is highly dependent on oversize forging machines and dies, which require high initial investments and operating costs. Second, the conventional manufacturing processes are normally lengthy and characterized by separate casting, forging, welding and milling, repeated heating, huge energy consumption, and high pollutant emissions. Third, thin-walled parts can be manufactured only by subtractive manufacturing, which is a hugely wasteful method with a material utilization rate lower than 10%. Fourth, it is difficult to manufacture functionally graded material (FGM) parts using conventional technologies [1].

At present, metal additive manufacturing has a broad range of applications. There are three main additive manufacturing methods, which respectively use laser, electron beam, and arc as the heat source [2-5]. Additive manufacturing of high-performance parts not only seeks to produce forged parts with stable and reliable microstructures and properties, but also pursues high efficiency and low cost. However, the industrialization of large, high-performance forging production is bottlenecked by the following problems:

• High energy beam (e.g. laser beam, electron beam or arc) manufacturing is virtually casting by welding deposition and does not involve forging. As high-performance parts are prone to metallurgical defects, warping and even cracking, large formed parts require high forming accuracy and can hardly attain desired mechanical properties for forgings when subject to dynamic loads. The anisotropy and unevenness of grain size, crystal orientation, and crystal structure cause great difficulty in internal structure and performance control [6-8].

• Unconstrained complex boundary and rapid alternate heating and cooling by a moving heat source cause uncertain and complex variations in thermodynamic conditions. The uncertainty and low controllability of the growth, microstructure, morphology, and size distribution of grains can affect the performance of finished parts [9-10].

• The aforementioned three techniques of high-energy beam additive manufacturing have advantages in terms of forming accuracy, forming efficiency, and operating cost, respectively. However, none of them meets all requirements related to performance stability and the three factors.

The CFMC additive manufacturing technology proposed in this paper can ensure high forming accuracy, high efficiency and low costs while offering high performance [11]. During production, continuous rolling was applied to the arc deposition's semi-solidification zone and finish milling was carried out one segment at a time [12]. Compared to laser additive manufacturing, CFMC additive manufacturing can offer higher deposition rate and formed parts with higher performance and stability at lower costs. Compared with electron beam additive manufacturing, it not only has advantages in performance of formed parts and cost, but also removes the constraints on the dimensions of parts being manufactured imposed by the size of the vacuum chamber.

Manufacturing process

The CFMC additive manufacturing process includes the following three steps:

- Welding deposition
- Micro-rolling
- Milling

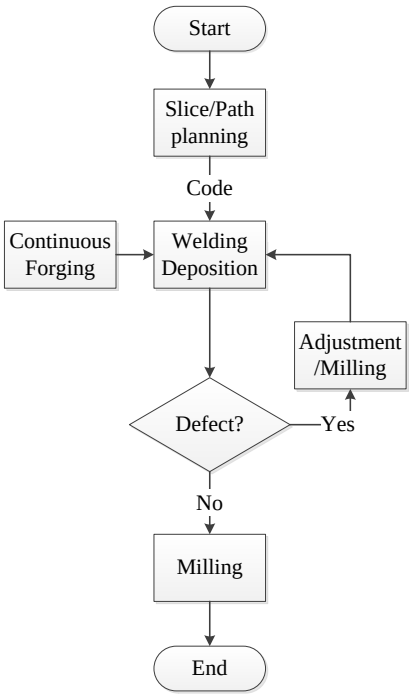

Fig. 1 Flow chart of CFMC additive manufacturing

First, proper process parameters are determined by process analysis of parts. Fig. 1 shows the flowchart of CFMC additive manufacturing. Slicing and path planning for the model are conducted using computer software [13]. A movement mechanism with a welding torch, which is controlled by the forming path code, is employed to perform welding deposition. Appropriate values are assigned to the process parameters, including wire feed rate, voltage, current, etc. Then deposition by wire-fed arc welding is performed, with argon being used as a shielding gas [14]. During welding deposition, heat is rapidly transferred to the substrate and the microstructure of the molten metal then evolves into a dendritic crystal or columnar crystal structure [15].

The second step is in-situ rolling, which uses a computer-controlled micro-rolling mechanism to apply a rolling force to the metal (Fig. 2). Then the metal undergoes plastic deformation and its columnar crystals break into fragments. Due to the effects of plastic deformation and heat input, the metal recrystallizes into equiaxed fine grains, and forgings are then obtained. Meanwhile, the on-line monitoring system performs data acquisition via the camera and data analysis and then feedbacks the results to the defect treatment module [16].

Next, the defect treatment mechanism treats the defects by means of automatic adjustment of process parameters, milling, etc. Then milling is performed to improve forming accuracy and roughness [17].

The composite manufacturing process employs two cooling sources: micro-roller and substrate. Normally, the first layer cools at the fastest rate and the rate of cooling decreases as the layer number increases. In order to ensure the cooling rate does not vary across layers, additional cooling equipment is needed as a complement.

This technology applies to a variety of metals, such as titanium alloys, stainless steels, nickel-based superalloys, austenite-bainite steels, and medium-carbon steel which has relatively low weldability [18].

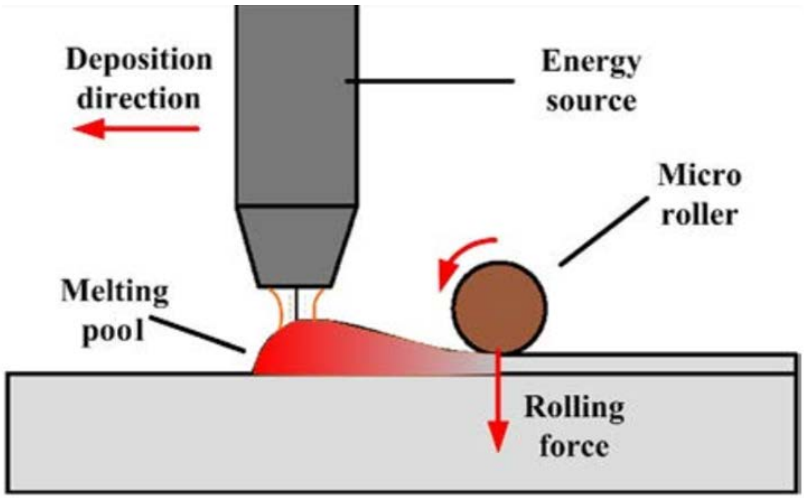

Fig. 2 Schematic of casting and forging

Equipment and devices

The equipment used in this technology includes a gantry-type arc welding and casting-forging-milling system equipped with numerical control system, an automatic positioning system with two executable units and an external control shaft, an automatic tool changer, and a hydraulic micro-forging system. The whole manufacturing system is highly flexible: it can perform welding deposition, forging, milling, and other operations, and the maximum dimensions and weight of workpiece it is capable of working are 5000mm*3000mm*2000mm and 15 tons, respectively (Fig. 3).

To guarantee the stable performance and reliable quality of the high-end parts fab ricated by additive manufacturing, online nondestructive testing must be conducted during welding deposition to examine the welding parameters and surface morphology of welding bead. During forming, infrared thermography and ultrasonic testing can be used to identify the size, location, nature, and quantity of defects in workpiece, such as surface and near-surface cracks, lack of fusion, voids, and slag inclusions. The characteristics of arc column and shape of welding pool can be detected using a system for image capture and computer graphic analysis and diagnosis. A real-time data acquisition system is used to monitor forming process parameters like arc current, voltage, track and velocity of motion of tool/workpiece, and wire feed rate [19].

We have used cameras and infrared devices to track and monitor the whole process of CFMC additive manufacturing. Fig. 4 shows the thermograms produced. It is clear from the figure that the specimen’s temperature field had a uniform distribution [20].

Fig. 3 Equipment for CFMC additive manufacturing

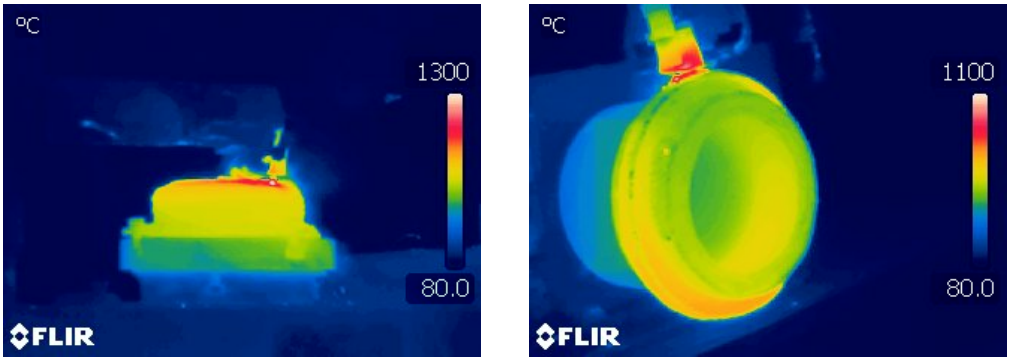

Fig. 4 Monitoring of CFMC additive manufacturing by infrared thermography

Numerical simulation

The stress variations in the freeform welding deposition (FWD) and Casting-Forging-Milling composite additive manufacturing technology (CFMC) specimens were simulated by ABAQUS. Fig. 5 shows the contours of maximum principal stress in the two specimens. It is clear from the figure that the maximum principal stress in the welding deposition specimens was primarily distributed in its central part and along the two long edges at the bottom. The CFMC additive manufacturing specimen had a greater surface area after forging and the deformation region created by forging mainly experienced compressive stress. The central part of the surface of the welding bead experienced compressive stress, while tensile stress occurred in the lateral parts. After forging, compressive stress arose in the region that was originally under tension after welding deposition. Vertically, plastic deformation occurred throughout the height of CFMC additive manufacturing. Given that tensile stress is the major cause of crack initiation and growth, it is reasonable to infer that micro-rolling can effectively inhibit initiation of cracks.

The evolution of the microstructures of the two specimens was modeled using MATLAB simulation program and the results are illustrated in Fig. 6 [21]. The rolling process increased dislocation density and induced dynamic recrystallization, which generated ultra-fine grains. This altered the developed columnar crystal structure resulting from welding deposition.

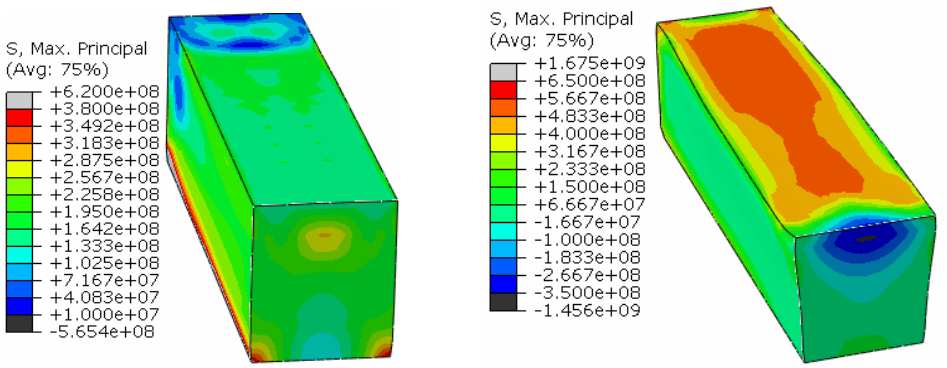

Fig. 5 Contours of maximum principal stress in FWD and CFMC specimens

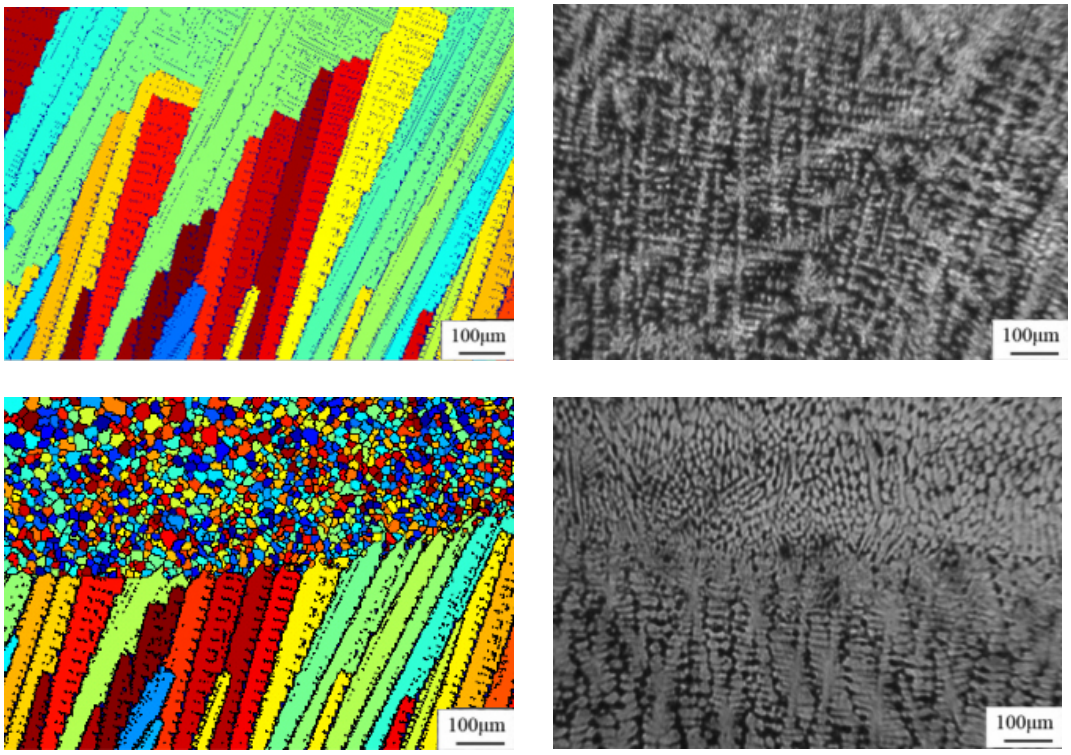

Fig. 6 Comparison of crystallization and crystal morphology in FWD and CFMC specimens

Experiments

The manufacturing process combining welding deposition with micro casting-forging was simulated using computer software. Then experiments were carried out to verify the simulation results. In the experiments, the welding direction and deposition direction were set as the x- and z-axis directions, respectively, and the horizontal direction perpendicular to the x-axis was the y-axis direction (Fig. 7). Different processes were then selected for different types of metals. Metal-inert gas (MIG) welding was selected for medium-carbon steel, titanium alloy, and stainless steel, while tungsten inert gas (TIG) welding was applied to nickel-based superalloy. Table 1-3 shows the process parameters for different metal.Proper insert shielding gases were used to protect the welding areas. A protective cover or atmosphere room was needed to prevent oxidization of titanium alloys. Then suitable heat treatment processes were selected for titanium alloy and nickel-based superalloy. Tensile testing at room temperature was performed on tensile specimens of medium-carbon steel, titanium alloy and nickel-based superalloy in accordance with the Chinese standard “Metallic Materials – Tensile testing – Part 1: Method of test at Room Temperature” (GB/T 228-2010), in order to measure their mechanical properties. Charpy impact tests at room temperature were conducted on specimens of titanium alloy

and nickel-based superalloy in accordance with the Chinese standard “Metallic materials – Charpy pendulum impact test method” (GB/T 229-2007). Later, the medium-carbon steel specimens manufactured by freeform welding deposition (FWD specimen) and CFMC additive manufacturing (CFMC specimen) were scanned using a scanning electron microscope for their microstructures.

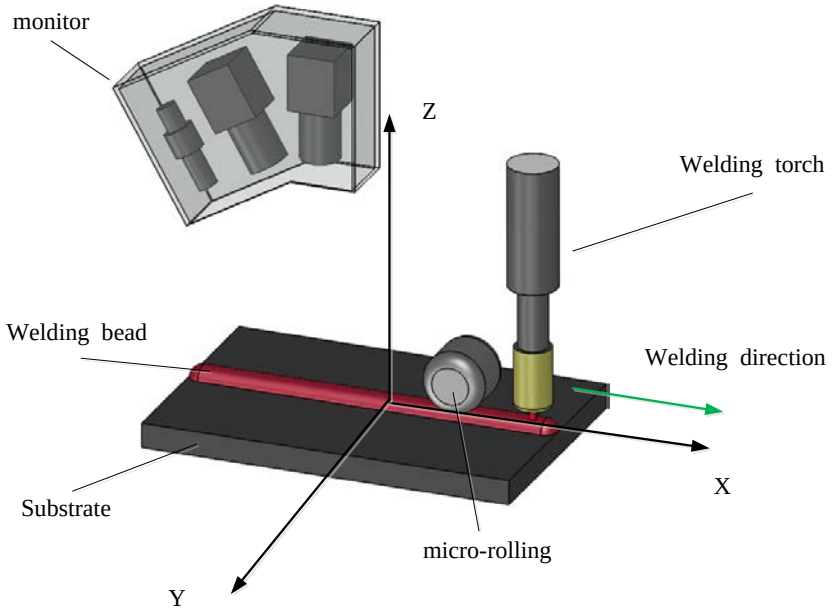

Fig. 7 A model of CFMC additive manufacturing

Table 1 Process parameters for forming of medium-carbon steels

Parameter	Value
Welding type	MIG
Wire feed rate	7.2 m/min
Welding speed	620 mm/min
Average voltage	27.3 V
Average current	241 A
Rolling force	3 kN

Table 2 Process parameters for forming of titanium alloys

Parameter	Value
Welding type	MIG
Wire feed rate	9.5 m/min
Welding speed	500 mm/min
Average voltage	27.3 V
Average current	241 A
Rolling force	5 kN
Annealing temperature	850℃

Table 3 Process parameters for forming of nickel-based superalloys

Parameter	Value
Welding type	TIG
Wire feed rate	1.3 m/min
Welding speed	160 mm/min
Average voltage	14 V
Average current	220 A
Rolling force	5 kN

Microstructural properties

Medium-carbon steel:

The microstructures of FWD and CFMC specimens were compared. Figs. 8a and 8c show the morphology of crystals in the FWD specimen. The X-section image (Fig. 8a) reveals the initial distribution pattern of crystal grains along the height of deposition: crystals grew from the vicinity of fusion lines, along the direction indicated by maximum temperature gradient, towards to the central part, resulting in a columnar microstructure. Along the fusion line, the columnar crystals became coarser with increasing height. They were approximately perpendicular to the fusion lines. Temperature gradients were large during welding cooling. The grains that were oriented in the same direction as the maximum temperature gradient grew rapidly. As crystals oriented in other directions grew at slower rates, they met the adjacent rapidly-growing grains before they developed well, and thus their growth was restrained. Ultimately, the columnar crystals showed roughly the same orientation. The coarse columnar crystals revealed in the figure were arranged in a dendritic pattern and had diameters of nearly 150 μm. As displayed by the Y-section of the FWD specimen (Fig. 8c), the initial crystal grains in different welding beads were largely columnar, but only those in the same welding bead were uniform in orientation, i.e. perpendicular to the corresponding fusion line. The orientation of columnar crystal in the Y-section varied between welding beads and the grains near each fusion line differed significantly in size.

Figs. 8b and 8d show the morphology of grains in the CFMC specimen. In the X-section (Fig. 8b), the originally columnar crystals nearly disappeared, because most of them had been shaped by micro-rolling to equiaxed grains. Compared to the initial grains in the X-section of the FWD specimen (Fig. 8a), the crystal grains in the CFMC specimen had much smaller sizes. The image of the Y-section (Fig. 8d) reveals that the original crystal growth pattern in which the parallel grains were perpendicular to the fusion lines had been heavily damaged, leaving a few small-sized columnar grains locally in the CFMC specimen. While the crystal grains in the regions within about 200 μm of the fusion lines maintained their initial columnar shape, crystals outside these regions were all broken and some of them exhibited shear distortion. A comparison of the Y-section images of the two specimens also reveals finer grain sizes in the CFMC specimen.

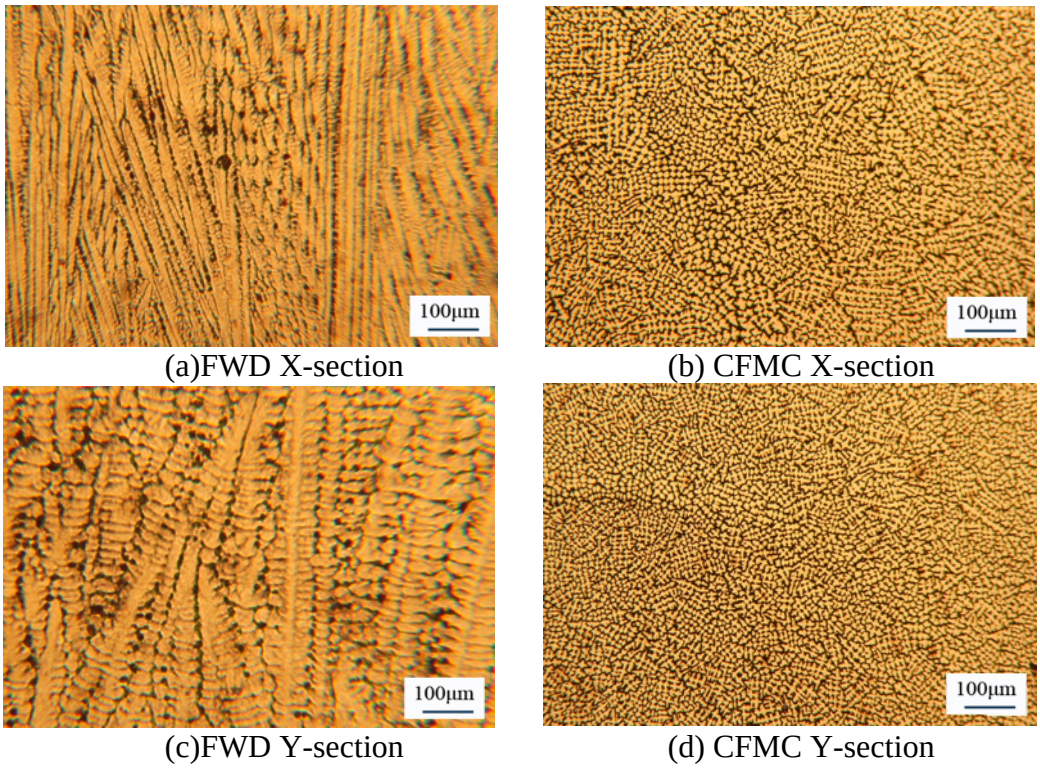

(a)FWD X-section (b) CFMC X-section

(c)FWD Y-section (d) CFMC Y-section

Fig. 8 Comparison of crystal grains in the FWD and CFMC

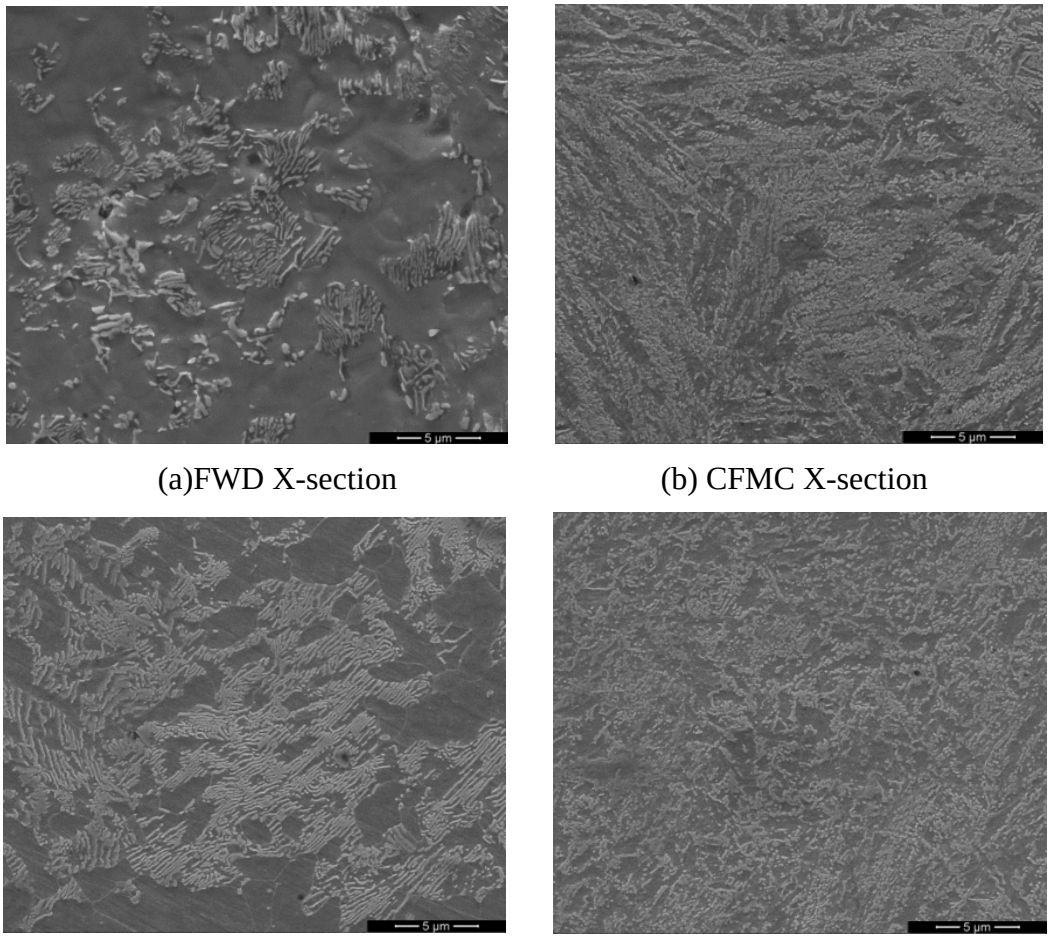

(a)FWD X-section (b) CFMC X-section

(c)FWD Y-section (d) CFMC Y-section

Fig. 9 SEM images showing the microstructures of FWD and CFMC specimens (10000x)

Furthermore, the X-section and Y-section of the specimens were scanned by SEM and interlayer spacing in the SEM images was measured with a micrometer, in order to analyze the distribution of carbide (Fig.9). In the X-section SEM image of the FWD specimen (Fig. 9a), the interlayer spacing largely fell within the range of 0.3 to 0.5 μm. In the Y-section SEM image of the FWD specimen (Fig. 9c), the interlayer spacing was mostly between 0.4 and 0.5 μm. The interlayer spacing criteria for distinguishing between pearlite, sorbite and troostite are as follows: pearlite: 150-450 nm; sorbite: 80-150 nm; and troostite: 30 to 80 nm. Therefore, the FWD specimen was composed primarily of pearlite, and the CFMC specimen was dominated by sorbate. No troostite was found.

Titanium alloys:

In arc welding, repeated heating can easily cause structural heterogeneity of welding beads. Therefore, proper heat treatment and deformation amount can play a significant role in ensuring structural homogeneity.

Titanium has two crystal structures: hexagonal close-packed structure, or α form, and body-centered cubic structure, or β form. The former structure occurs at room temperature and then changes to the latter through at 882 °C or above as a result of phase change. The microstructures of titanium alloys split into the following types: α+β equiaxed microstructure, α+β duplex microstructure, and α+β basketweave microstructure, and Widmanstatten microstructure.

The experimental research found that titanium alloy specimen that remained undeformed after annealing at 850°C had Widmanstatten and locally basketweave microstructures. The specimen that was deformed by rolling exhibited no α phase at crystal boundaries, but increased equiaxed α phase; its interior part showed a α+ basketweave + transformed β triplex microstructure, which can give the alloy good comprehensive performance.

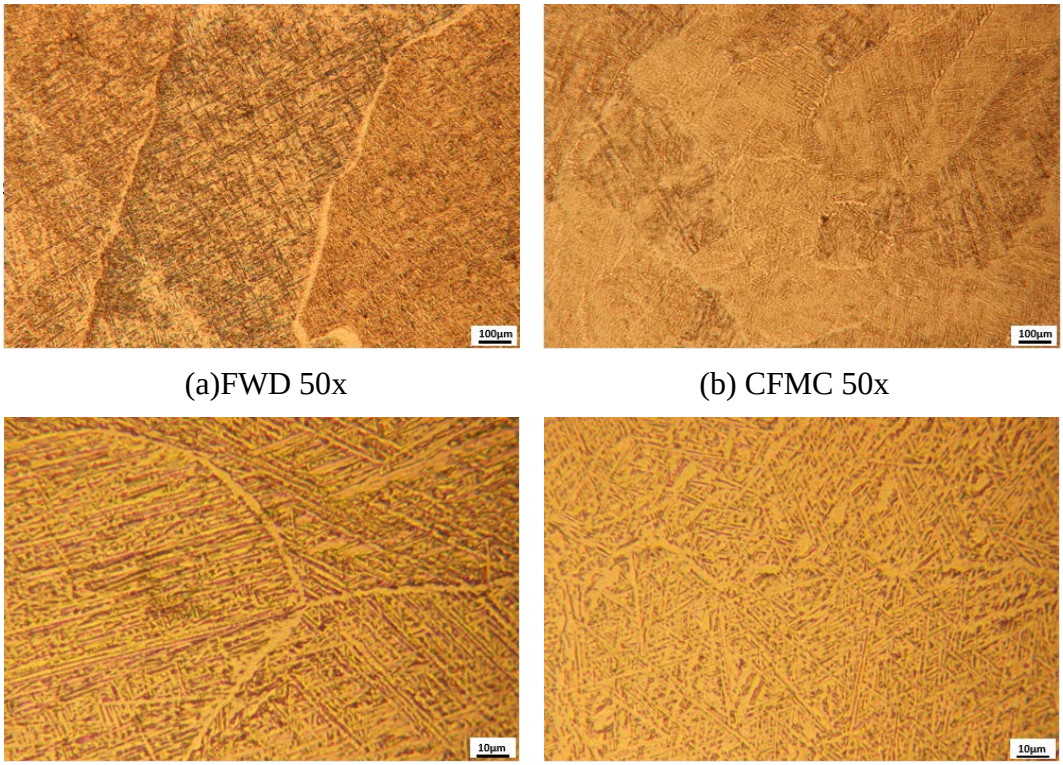

(a)FWD 50x (b) CFMC 50x

(c)FWD 50x (d) CFMC 50x

Fig. 10 Comparison of crystalline phases of titanium alloys

Fig. 10 demonstrates that the undeformed specimen had a coarse columnar crystal microstructure and the columnar crystal had a thick α phase boundary. In terms of microstructure, the continuous α phase along this boundary contained parallel α clusters that grew inward, a typical Widmannstatten microstructure. The main contributor to this microstructure is the insufficient heat treatment of the β phase titanium alloy or inadequate amount of deformation. As each heating process during welding is equivalent to a post-heat treatment, the welding area's temperature tended to exceed the point at which the β-phase transformation began, thus facilitating the formation of the Widmannstatten microstructure. In contrast, the temperature in the heat-affected region was far below the phase transformation point, allowing the crystal grains within it to continue growing. Therefore, the Widmannstatten microstructure was not distributed throughout undeformed specimen. The annealing at 850 ℃only homogenized the interior microstructure, but did not remove the β-phase coarse grains that spread throughout the height of the specimen and the Widmannstatten microstructure. Since the Widmannstatten microstructure has poor plasticity, it is necessary to remove it during heat treatment of titanium alloys.

The CFMC specimen displayed finer equiaxed β-phase grains and no continuous α phase along grain boundary. Its microstructures included uniformly distributed equiaxed α and transformed β microstructures. The α microstructure outnumbered the transformed β microstructure and the latter showed smaller interlayer spacing. Overall, the CFMC specimen consisted primarily of duplex microstructures, which combine the advantages of equiaxed and basketweave microstructures and guarantee high plasticity and toughness.

Nickel-based superalloys：

Nickel-based superalloy wires were tested by arc welding deposition and CFMC separately. The specimens produced by the two processes were compared in terms of structural and mechanical properties. Fig. 11 reveals that the dendritic crystal structure in the interior of the CFMC specimen was damaged and the slender columnar grains that were observed in the FWD specimen were replaced by equiaxed grains as a result of dynamic recrystallization.

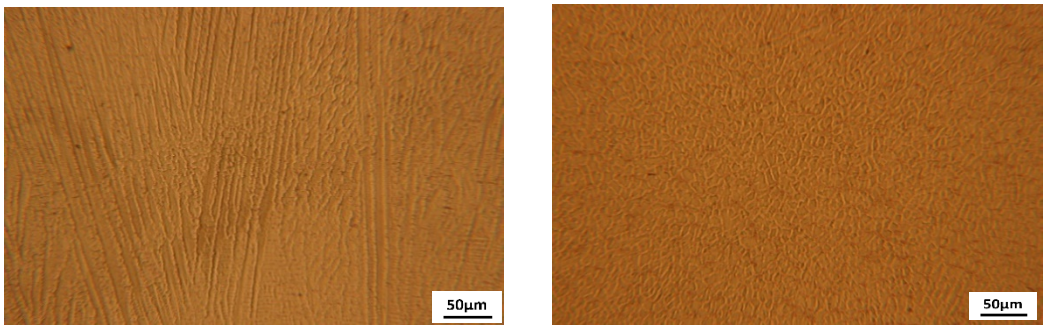

(a)FWD (b)CFMC

Fig. 11 Comparison of crystalline phases of nickel-based superalloy specimens produced by FWD and CFMC

Mechanical properties

medium-carbon steel

Table 4 Mechanical properties of medium-carbon steel

Specimen	Tensile strength σ_b (MPa)	Yield strength $\sigma_{0.2}$ (MPa)	Elongation δ (%)	Hardness (HBS)	Shrinkage ψ (%)	Impact toughness ($J \cdot mm^{-2}$)
Standards for forgings	835	490	10	229-285	40	44
FWD	688	382	13	290	-	-
CFMC	973	644	18	301-308	46	47.5

The mechanical properties of forgings listed in the table above are sourced from the Chinese standard "Steel forgings for aviation" (HB 5024-89).

The rolled parts outperformed those obtained by welding deposition in mechanical properties. Compared to the standards for forgings, the rolled parts had significantly improved mechanical properties, with a 16.5% increase in, 31.4% increase in yield strength, 80% increase in elongation, 8.1% increase in hardness, 15% increase in shrinkage, and 8.0% increase in impact toughness.

Mechanical properties of titanium alloy

After annealing at 850 ℃, the titanium alloy attained optimal mechanical properties. As shown in the table below, the mechanical properties of the titanium alloy specimens created by FWD were above the standard values for forgings except yield strength. The specimens obtained from CFMC + heat treatment (annealing at 850 ℃) exhibited the best mechanical properties. Their tensile strength, yield strength, elongation, and impact roughness increased 18.3%, 16.7%, 57%, and 61.1%, respectively, from those of forgings, and were up 8.5%, 17.8%, 37.7%, and 39.2% from the FWD specimens.

Table 5 Mechanical properties of titanium alloy

Specimen	Tensile strength σ_b (MPa)	Yield strength $\sigma_{0.2}$ (MPa)	Elongation δ (%)	Impact toughness ($J \cdot mm^{-2}$)
Standards for forgings	895	828	10	35
FWD	976	820	11.4	40.5
CFMC + heat treatment	1059	966	15.7	56.4

The mechanical properties of forgings listed in the table above are sourced from the Chinese standard "Titanium and titanium alloy forgings" (GB/T 25137-2010).

Table 6 Mechanical properties of nickel-based superalloy

Specimen		Tensile strength σ_b (MPa)	Yield strength $\sigma_{0.2}$ (MPa)	Elongation δ (%)	Shrinkage ψ (%)	Impact toughness ($J \cdot mm^{-2}$)
Standards for forgings	X-axis	1253	1034	12	15	
	Y-axis	1241	1034	10	12	39*
	Z-axis	1241	1034	6	8	
FWD	X-axis	724	446	19	-	43
	Y-axis	740	450	15	-	41
	Z-axis	674	449	18	-	42
CFMC + heat treatment	X-axis	1302	1108	16	26	51
	Y-axis	1343	1137	17	21	56
	Z-axis	1347	1165	16	-	53

The mechanical properties of forgings presented above are sourced from the Chinese standard “GH4169 alloy bars, forgings and rings” (GB/T 25137-2010), except the value of impact roughness, which is provided by the standard “GH4169 alloy rods for aerospace”.

The high tensile and yield strengths of the FWD specimens of nickel-based superalloy suggest relatively high plasticity. Their average impact roughness was 7.7% higher than the standard value for forgings. The specimens obtained from CFMC + heat treatment showed substantial improvements in comprehensive mechanical properties. The heat treatment process included heating at 1090 ℃ for 1-2 hours, air cooling at +950 ℃ for 1 hour, air cooling at +72 ℃ for 8 hours, furnace cooling at a rate of 50 ℃/h to 620 ℃, and air cooling for 8 hours. In this process, the specimen went through homogenization, solution hardening, and two-stage aging treatment. After the heat treatment, the interior crystal grains in the CFMC specimens changed to aquiaxed grains of varying sizes through recrystallization. The recrystallization process was accompanied by crystal twinning. Due to the presence of aquiaxed crystals, the specimens can attain excellent comprehensive mechanical performance with higher tensile strength, yield strength, toughness, and hardness than corresponding standards for forgings.

Conclusions and future works

A transition piece for aviation made of medium-carbon steel

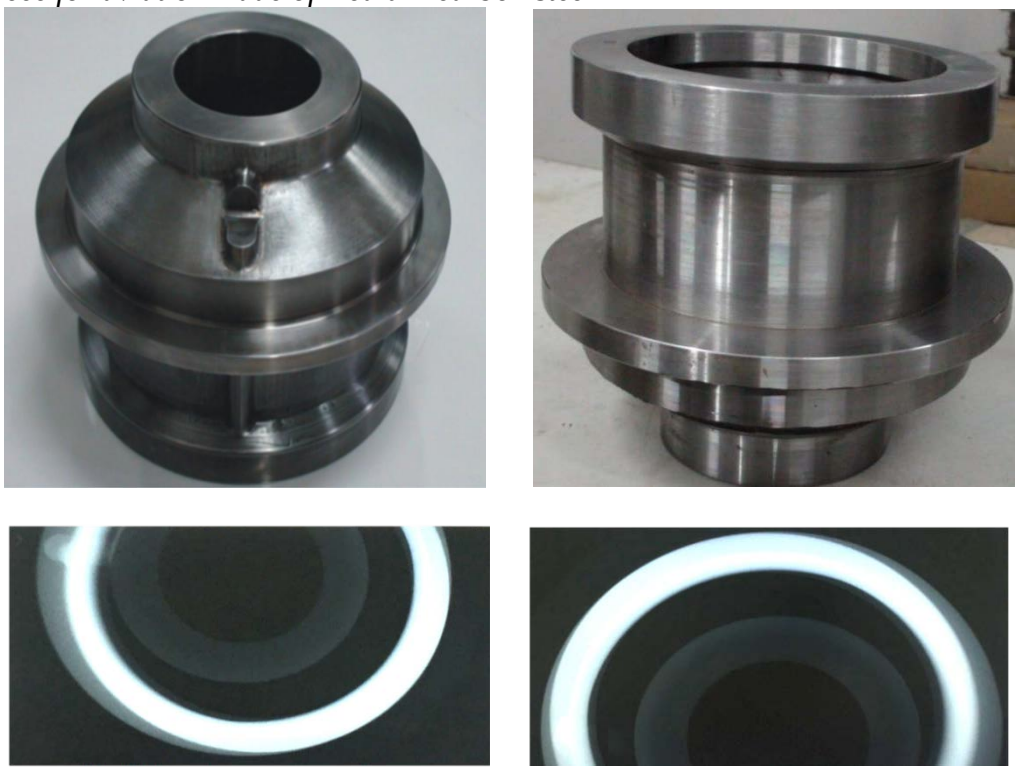

Fig. 12 A transition piece for aviation and its X-ray images

Fig. 12 shows a transition piece for aero-engines developed in cooperation with AECC Xi'an Aero-Engine Ltd. Due to their non-uniform wall thickness, transition pieces manufactured by the traditional investment casting are prone to cracking, loosening, and deformation and likely to have high porosities. As a result, the manufacturing process has an extremely low yield of less than 10%. The transition piece shown in the figure above is produced by the CFMC additive manufacturing technology proposed in this study. The X-ray testing reveals no flaw in it. This CFMC part is proven to be micro-grained and super-strong and its metallurgical quality meets Ukraine's strict standard for aero-engine testing.

Titanium alloy aeronautical part

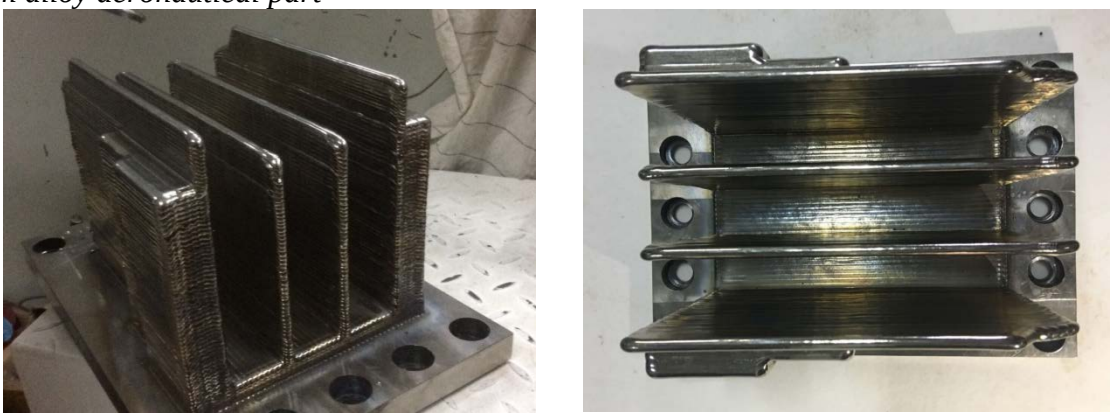

Fig. 13 Titanium alloy aeronautical part before milling

(a) austenite-bainite steel frog

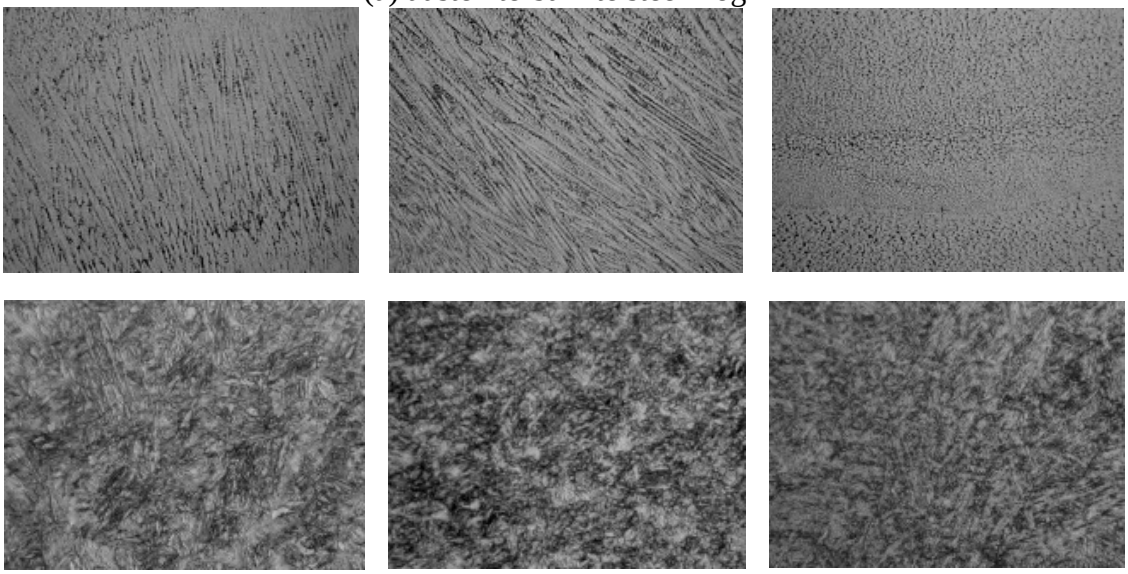

(b)Free annealing (c)Austempering and tempering (d)Rolling and heat treatment

Fig. 14 An austenite-bainite steel frog and microstructures of steel

This frog is intended for switches on high-speed railways. It is manufactured from austenite-bainite steel by the CFMC additive manufacturing technology and has better properties than forgings. This type of frog has been applied in practice. The figure above shows that the crystal grains resulting from rolling and heat treatment are finer than those from austempering and tempering.

Other sample pieces

(a) Stainless steel propeller

(b) An aeronautical part from high-silicon aluminum alloy

(c)A highly-skewed integrated impeller

(d) Alloy drag plate

Fig.15 Sample pieces

Advantages:

• It performs casting and forging simultaneously and can produce forgings with a hyperfine aquiaxed grain structure.

CFMC can reduce the anisotropy of parts' interior structures and increase their toughness, which guarantee uniformity of materials and thereby improve components' fatigue life and reliability. It is able to produce not only thin-walled metal parts, but also parts with non-uniform wall thicknesses. As the most accurate forging methods can only produce fine-grain metals, the conventional techniques of metal additive manufacturing are incapable of manufacturing forgings.

• Less or no use of huge traditional casting and forging equipment

In traditional machinery manufacturing, casting, forging, welding, and milling units

CFMC will combine the separate units for casting, forging, welding, and milling in conventional heavy-equipment manufacturing into an integrated manufacturing unit, thus achieving light-equipment manufacturing with shorter processes, higher energy efficiency, and lower pollutant production. The computer-controlled forming paths help significantly reduce equipment investment and material cost.

• High rate of material utilization

Using metal wires as the raw material, CFMC can guarantee a rate of material utilization higher than 70%. The prices of wire materials are about only 1/10 of those of powder materials, which are widely used in common additive manufacturing techniques that involve laser melting of powder.

• High efficiency and low cost of arc

The most popular techniques of metal additive manufacturing all use laser and powder based methods. Lasers are the most expensive devices used in metal additive manufacturing and most lasers need to be imported. For a given power level, using arc as the heat source can reduce cost ten-fold compared to the cost of laser-based manufacturing.

• Shorter production cycles

Because CFMC can control parts' dimensions, shape, microstructures and properties, it can offer a deposition rate of 5-15 kg/h and a double-wire deposition rate of 20-30 kg/h. Thus a record decrease of 60% in lead time can be achieved: while it takes more than three months to manufacture a two-ton metal forging in the past, CFMC needs only about 10 days.

• Energy-efficient green manufacturing

As the production equipment needs a power supply of only 50 kW, its energy consumption per unit time is about only 2‰ of a huge pressing machine's. Therefore, CFMC can provide an effective solution to the problems of huge energy consumption and high pollutant emissions in traditional machinery manufacturing and help open up a new era of green manufacturing.

Further work will focus on optimizing forging parameter, improving milling efficiency, and manufacturing titanium alloy aeronautical parts in atmosphere room and nickel-based superalloy parts for aero-engines.

References

[1] Niendorf, T., Leuders, S., Riemer, A., Brenne, F., Tröster, T., & Richard, H. A., et al. (2014). Functionally graded alloys obtained by additive manufacturing †. Advanced Engineering Materials, 16(7), 857–861.

[2] Kruth, J. P., Froyen, L., Vaerenbergh, J. V., Mercelis, P., Rombouts, M., & Lauwers, B. (2004). Selective laser melting of iron-based powder.Journal of Materials Processing Technology, 149(1–3), 616-622.

[3] Murr, L. E., Gaytan, S. M., Ramirez, D. A., Martinez, E., Hernandez, J., Amato, K. N., ... & Wicker, R. B. (2012). Metal fabrication by additive manufacturing using laser and electron beam melting technologies. Journal of Materials Science & Technology, 28(1), 1-14.

[4] Wang, F., Williams, S., Colegrove, P., & Antonysamy, A. A. (2013). Microstructure and mechanical properties of wire and arc additive manufactured ti-6al-4v. Metallurgical & Materials Transactions A, 44(2), 968-977.

[5] Frazier, W. (2014). Metal additive manufacturing: A review. Journal of Materials Engineering & Performance, 23(6).

[6] Liao, H., Fu, P., Peng, L., Li, J., Zhang, S., & Hu, G., et al. (2017). Microstructure and mechanical properties of laser melting deposited gw103k mg-re alloy. Materials Science & Engineering A, 687, 281-287.

[7] Zhu, Y., Tian, X., Li, J., & Wang, H. (2014). Microstructure evolution and layer bands of laser melting deposition ti–6.5al–3.5mo–1.5zr–0.3si titanium alloy. Journal of Alloys & Compounds, 616(2), 468-474.

[8] Lawrence, Murr, Sara, Gaytan, Diana, & Ramirez, et al. (2012). Metal fabrication by additive manufacturing using laser and electron beam melting technologies. Journal of Materials Science & Technology, 28(1), 1-14.

[9] Martina, F., Roy, M. J., Szost, B. A., Terzi, S., Colegrove, P. A., & Williams, S. W., et al. (2016). Residual stress of as-deposited and rolled wire+arc additive manufacturing ti–6al–4v components. Materials Science & Technology, 160224043911007.

[10]Martina, F., Colegrove, P. A., Williams, S. W., & Meyer, J. (2015). Microstructure of interpass rolled wire + arc additive manufacturing ti-6al-4v components. Metallurgical & Materials Transactions A, 46(12), 6103-6118.

[11]Zhang, H ., Wang, X., Wang, G., & Zhang, Y. (2013). Hybrid direct manufacturing method of metallic parts using deposition and micro continuous rolling. Rapid Prototyping Journal, 19(6), 387-394.

[12] Wohlers T, M（2017）; Wohlers report 2017, US: Wohlers Associates, Inc, 2017.

[13] Ding, D., Pan, Z., Cuiuri, D., & Li, H. (2015). A multi-bead overlapping model for robotic wire and arc additive manufacturing (waam). Robotics and Computer-Integrated Manufacturing, 31(C), 101-110.

[14] Carroll, B. E., Palmer, T. A., & Beese, A. M. (2015). Anisotropic tensile behavior of ti–6al–4v components fabricated with directed energy deposition additive manufacturing. Acta Materialia, 87, 309-320.

[15] Zhang, H. (2016). Method for manufacturing metal parts and molds and micro-roller used therefor.

[16] Zhan, Q., Liang, Y., Ding, J., & Williams, S. (2017). A wire deflection detection method based on image processing in wire + arc additive manufacturing. International Journal of Advanced Manufacturing Technology, 89(1-4), 755-763.

[17] Xiong, X., Zhang, H., & Wang, G. (2008). A new method of direct metal prototyping: hybrid plasma deposition and milling. Rapid Prototyping Journal, 14(1), 53-56.

[18] Fu, Y., Wang, G., Zhang, H., & Liang, L. (2016). Optimization of surface appearance for wire and arc additive manufacturing of bainite steel.International Journal of Advanced Manufacturing Technology, 1-13.

[19] Ding, Y., Warton, J., & Kovacevic, R. (2016). Development of sensing and control system for robotized laser-based direct metal addition system.Additive Manufacturing, 10, 24-35.

[20] Zhang, H. O., Rui, W., Liang, L., & Wang, G. L. (2016). Hdmr technology for the aircraft metal part. Rapid Prototyping Journal, 22(6), 857-863.

[21] Zhou, X., Zhang, H., Wang, G., Bai, X., Fu, Y., & Zhao, J. (2016). Simulation of microstructure evolution during hybrid deposition and micro-rolling process. Journal of Materials Science, 51(14), 6735-6749.